Received: 15 January 2019 | Revised: 16 March 2019 | Accepted: 5 April 2019

DOI: 10.1002/we.2353

RESEARCH ARTICLE

WILEY

Analysis and study of two-dimensional parameter bifurcation of wind power farms and composite loads

Abdelaziz Salah Saidi[1,2] | Marwa Ben Slimene[3] | Mohamed Arbi Khlifi[4] | Mohammad Fazle Azeem[1,5] | Salah Al Ahmadi[4] | Azzedine Draou[4]

[1] Department of Electrical Engineering, King Khalid University, Abha, Saudi Arabia

[2] Electric Systems Laboratory, National Engineering School of Tunis (ENIT), Tunis, Tunisia

[3] College of Computer Science and Engineering (CCSE), University of Hail KSA, Hail, Saudi Arabia

[4] Department of Electrical Engineering, Islamic University in Madinah, Madina, KSA

[5] Department of Electrical Engineering, Aligarh Muslim University, Aligarh, UP, India

Correspondence
Mohamed Arbi Khlifi, Department of Electrical Engineering, Islamic University in Madinah, Madina, KSA.
Email: mohamedarbi.khlifi@issatm.rnu.tn

Abstract

This study focuses on the stability of power system based on codimension-two bifurcation theory. In this paper, we investigate the impact of load modeling on permissible wind power generation margins in distribution networks. The study considers codimension-two bifurcations of equilibria and limit cycles in wind power systems depending on varying two parameters simultaneously. The principle parameter is the wind power generation, and the other parameter depends on the different types of loads. The types of loads are ZIP, exponential recovery, dynamic induction loads, and composite load models. To study the effects of the induction motor loads, the proportion of the static component in the motor load is changed and assessed with respect to their mechanical loads. Wind generation margin boundaries are traced, and saddle-node, Hopf, and limit-induced bifurcation branches are obtained, delimiting the stable and unstable operating regions in the parameter space. The analysis presented in this paper can pave the way for determining methods for improving and monitoring these margins with consideration to the system parameters and load composition.

KEYWORDS

composite load, distribution network, power system stability, two-parameter bifurcation analysis, wind power generation

1 | INTRODUCTION

In modern power systems, the increasing level of wind power penetration has imposed new challenges to transmission and distribution system to maximize the use of power, while maintaining high levels of reliability and security of the system. Despite the advancement in wind turbine technology and improvement in active control systems for transmission and distribution networks,[1,2] grid voltage stabilization is still the prime concern for system operators. In many studies, the risk of voltage collapse is used as an indicator for permissible wind penetration level. For distribution networks, many identified problems are related to the load representation in simulation tools. One aspect is that distribution network loads represent the behavior of different end-user components. Therefore, it may exhibit complex static and dynamic responses to system disturbances.

- We investigate the impact of load modeling on permissible wind power generation margins in distribution networks.
- We consider codimension-two bifurcations of equilibria and limit cycles in wind power systems depending on two parameters varying simultaneously. The principle parameter is the wind power generation, and the other parameter depends on the different types of loads.
- We consider static and composite load models. Motor loads are assessed with respect to their mechanical loads. Wind generation margin boundaries are traced, and saddle-node, Hopf, and limit-induced bifurcation branches are obtained, delimiting the stable and unstable operating regions in the parameter space.

Drive loads in power system are quite diverse and complex, which intensifies nonlinear dynamic characteristics. Bifurcation theory is an effective tool to investigate the structural stability of nonlinear dynamic systems.

A composite load structure has been recommended by Western Electricity Coordinating Council (WECC) standards,[3] consisting of multiple loads connected to a single bus, namely, static, motor, and dynamic with exponential recovery load as shown in Figure 1. Although such composite load structures augmented to wind farm models may complicate the overall system simulation model. Many studies[4-6] have shown the importance of such detailed modeling in improving the reliability of simulation. Researchers have investigated[7-17] the voltage stability in distribution networks integrating wind farms, using different load model representations. Khlifi[7] has shown that voltage instability occurred only due to the presence of the induction motor load. In Gu et al,[8] the line current of the IEEE 39 bus system with exponential and ZIP models has a more serious negative impact on voltage stability than the other limitations taken into account. In Zheng et al,[9] the authors have shown that power system stabilizers may remove the Hopf bifurcations (HBs) and improve the system stability with large-scale variable-speed wind turbines. In Linh et al,[10] an efficient method has been presented for determining the maximum permissible PQ loadability of a distribution network for wind power generation. In Saïdi et al,[11] the authors have used wind generation as a bifurcation parameter for determining the stability margin, based on static and dynamic continuation power flow (CPF) techniques. The study in Toma et al[12] has demonstrated that voltage dependency of load has increased the saddle-node bifurcation point, but with the cost of much lower voltage values at system buses. In all the above studies, most of wind power system voltage stability studies carried out by using bifurcation theory are single-parameter bifurcation analysis.

A power system is basically a multiparameter nonlinear dynamic system. This leads a complex behavior, and a consensus is still lacking about the mechanisms of voltage instability in a power system. A detailed information about the effects of load characteristics on the voltage stability is of significant theoretical value. Very few researches, without detailed analysis, are mentioned in literature[18] that involve two-parameter bifurcation analysis of wind power system. In Shaofeng et al,[19] studies shows that multiparameter bifurcation needs more computation for system parameters to the power system voltage stability in comparison with single-parameter analysis. In earlier studies, researchers had mainly implemented a multiparameter bifurcation analysis method. The effects of single load parameters on the bifurcation point under the codimension-one condition have been explored, and voltage instability has been analyzed. In order to reflect the voltage instability mechanism and margin more accurately, the overall considerations including multiple parameters should be taken care. In the previous studies,[20,21] the effects of load characteristics on voltage instability have been studied based on codimension-two bifurcation analysis method by changing the fraction of the static component in the polynomial load model. The bifurcation points have been searched using a multiparameter bifurcation theory. It has revealed various phenomena that cannot be found using one-parameter bifurcation theory. Multiparameter bifurcation theory has been proposed in previous studies.[22,23] The active and reactive power of the bus bar have been used as the bifurcation parameters to study system stability in a two-generator and five-test bus system. Ma et al[24] have inferred that a surge in reactive compensation in wind power farms could remarkably quash saddle-node bifurcation (SNB) and thus improve the system's injection power limit. Li et al[25] have found that a delay in oscillatory instability of HB for wind power farms could be achieved by increasing line admittance. Jiang et al[26] have applied multiparameter bifurcation theory to analyze a multimachine power system and resolved that the oscillatory instability could not be delayed always by increasing the excitation reference voltage of any generator in the system. Whereas, using static VAR compensators (SVCs) as a supplementary control can favorably increase the system damping, delay the HB point, and significantly increase the system's dynamic load margin.

In this paper, we utilize a composite load model for assessing wind power penetration in a distribution network. The composite load comprise of static, dynamic, and exponential recovery load components are described in Section 2. Moreover, motor loads are assessed with respect to their mechanical loads, and the wind farm consists of variable speed induction generators that are also presented in Section 2. Section 3 presents two models of the network: a differential algebraic equation (DAE) model with a voltage-dependent static load and a DAE model with a fully dynamic load. Section 4 analyzed codimension bifurcation using the developed differential algebraic representation, and the study is based on the determination of bifurcation points. Section 5 describes the proposed assessment methodology. Simulation results, comparison for the four models in terms of permissible wind penetration, and discussions are presented in Section 6. The bifurcation points indicate the load-generator dynamic interaction and the network permissible wind power penetration. Finally, conclusions are relegated to Section 7.

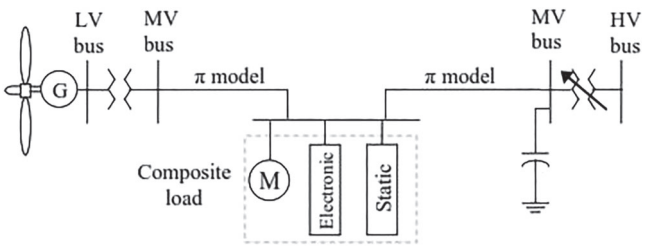

FIGURE 1 A nonlinear distribution network structure and its composite load model

2 | MATHEMATICAL DESCRIPTION OF THE POWER SYSTEM AND COMPOSITE LOAD MODEL

The WECC load modeling task force[3] has made perennial efforts in developing a composite load model that can represent the behavior of different end-user components in power systems. Composite load responses are typically dominated by the dynamic behavior of LTC transformers, induction motors, and thermostatically controlled loads. The modeling structure of the composite load model recommended by the WECC load modeling task force is illustrated in Figure 1. The composite load is a combination of static and dynamic load components. It consists of an induction motor load with a constant *PQ* load in parallel[3,27] with an exponential recovery load and a ZIP load. The total power consumed by the composite load is given by,

$$P_{\text{comp}} = P_{\text{ZIP}} + P_{\text{IM}} + P_{\text{rec}} \tag{1}$$

2.1 | Mathematical description of the wind generator and network models

The wind turbines are based on DFIGs. These are represented by a reduced-order model with internal electromotive forces, given as $\overline{E}' = E'e^{i\delta}$, with a transient reactance[28] and is widely applied in the investigation of power systems. A simplified model for the dynamics of the control loop converter can be employed.[11,29] The converter is modelled by an ideal current source. The direct current i_{rd} is used for the rotor speed control, whereas quadrature current i_{rq} is used for the voltage control. The pitch angle θ_p is used for maximum power control. Single-mass model is used to represent inertial dynamics of all rotating masses. The magnitude and the angle of the internal generator voltage $E'$and δ, the rotor currents (i_{rd}, i_{rq}), the pitch angle θ_p, and the rotor slip s^D are the state variables.

The distribution lines and transformers are modeled with a common branch model, consisting of a standard π transmission line with a transfer admittance given as $^{-}_{ij} = G_{ij}+jB_{ij}$ and an equivalent charging admittance, $^{-}_{Cij} = G_{Cij}+jB_{Cij}$. The LTC controls the secondary voltage allowing the tap ratio to change in steps with step-size Δm. The step change represented by the discrete model mention in Milano,[30] and given as below:

$$m_{k+1} = m_k + \Delta m R \tag{2}$$

The relay type function R is given as

$$R = \{\, 1 \;\text{ if } u - u_{\text{ref}} \succ \Delta u \; -1 \text{ if } u - u_{\text{ref}} \prec -\Delta u \tag{3}$$

Here, u is the input voltage; u_{ref} is the reference voltage, and Δu is the error tolerance. For the transformer, the π-model parameters are functions of the transformer tap ratio m and the impedance$^{-}_{T}+jx_T$. They are given as $\overline{Y}_{ij} = m/\overline{z}$, $\overline{Y}_{Cij} = (1-m)/\overline{z}$, and $\overline{Y}_{Cji} = m(1-m)/\overline{z}$.

2.2 | Mathematical description of the composite load model

In the composite load model, to obtain greater control over the parameters of the dynamic and static characteristics, the static load model ZIP is connected in parallel with the induction machine as shown in Figure 1. P_1+jQ_1 is the static load, and P_d+jQ_d is the load of the dynamic induction motor.

2.2.1 | Static load model

Usually power consumption by static load models is dependent on voltage and frequency. The voltage dependency is articulated in a polynomial or exponential form and frequency dependency in linearized form. These two dependencies are multiplied and given as Equations (2) and (3). This model known as the ZIP model.[31]

$$P_{\text{zip}} = P_o\left[a_1\left(\frac{V}{V_o}\right)^2 + a_2\left(\frac{V}{V_o}\right) + a_3\right](1 + a_{fP}\Delta f) \tag{4}$$

$$Q_{\text{zip}} = Q_o\left[b_1\left(\frac{V}{V_o}\right)^2 + b_2\left(\frac{V}{V_o}\right) + b_3\right](1 + a_{fQ}\Delta f) \tag{5}$$

where,V_o,P_o, and Q_o are the nominal operating conditions of the system; α_{fP} and α_{fQ} are the frequency dependency parameters. The coefficients $a_{i\,=\,1,2,3}$ and $b_{i\,=\,1,2,3}$ are the load model parameters and satiating the equality, $a_1+a_2+a_3 = b_1+b_2+b_3 = 1$. They specify the division of nominal power into constant power, constant current, and constant load impedance components. Similar relation is valid for the reactive power. The values for the coefficient of the model for different load components are available in the previous studies.[16,17,31-50]

2.2.2 | Dynamic load

The use of static instead of dynamic motor models is commonly suspected to be a major source of errors in simulation results. The dynamic load models considered in our work are the induction motor and exponential recovery load. They are discussed below.

Machine load

The squirrel cage induction machine (SCIM) model has been considered, and its steady-state equivalent circuit is shown in Figure 2. In stability analysis, the SCIMs are modeled by reduced-order model neglecting the stator flux dynamics.[32] The model can be represented by transient voltage source lagging behind transient impedance as shown in Figure 2.

Major portion of the dynamic loads of a power system constitutes SCIMs. The influence of these machines on transient voltage stability is considered to be noteworthy.[33] The studies in Borghetti et al[34] have described the induction machine model used in power system voltage stability studies. The stator flux linkage transient is neglected ($\psi_{qs} = \psi_{ds} = 0$). This reduces the fifth-order model to a simplified third-order model (Figure 3). The dynamic behavior of the induction machine is described by following three nonlinear differential equations:

$$\begin{aligned}
\dot{E}_d^{'} &= w_b s E_q^{'} - \left(E_d^{'} + \left(X_o - X^{'}\right) I_q\right)/T_o^{'} \\
\dot{E}_q^{'} &= -w_b s E_d^{'} - \left(E_q^{'} - \left(X_o - X^{'}\right) I_d\right)/T_o^{'} \\
\dot{s} &= (T_m(s) - T_e)/(2H_m) \\
V_{sd} - E_d^{'} &= R_s I_{sd} - X^{'} I_{sq} \\
V_{sq} - E_q^{'} &= R_s I_{sq} + X^{'} I_{sd}
\end{aligned} \tag{6}$$

and the two stator algebraic equations as given by equations:

$$\begin{aligned}
\dot{E}_d^{'} &= \omega_b s E_q^{'} - \left(E_d^{'} + \left(X_o - X^{'}\right) I_q\right)/T_o^{'} \\
\dot{E}_q^{'} &= -\omega_b s E_d^{'} - \left(E_q^{'} - \left(X_o - X^{'}\right) I_d\right)/T_o^{'} \\
\dot{s} &= (T_m(s) - T_e)/(2H_m) \\
V_{sd} - E_d^{'} &= R_s I_{sd} - X^{'} I_{sq} \\
V_{sq} - E_q^{'} &= R_s I_{sq} + X^{'} I_{sd}
\end{aligned} \tag{7}$$

where,

$$\begin{aligned}
X_o &= X_s + X_m, \\
X^{'} &= X_s + (X_r X_m / X_r + X_m), \\
T_o^{'} &= (X_r + X_m)/\omega_b R_r
\end{aligned} \tag{8}$$

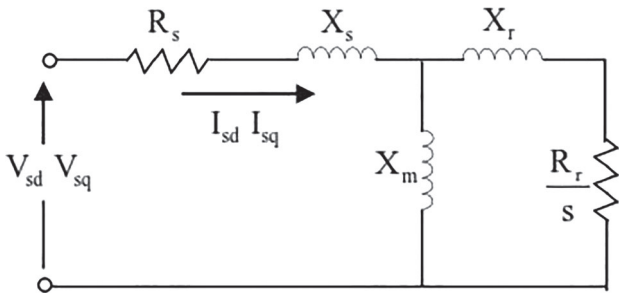

FIGURE 2 Induction machine model

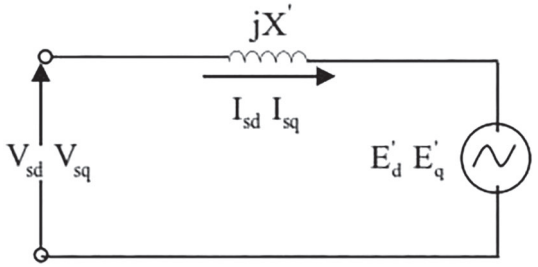

FIGURE 3 Third-order equivalent circuit of the induction machine model

where E'_d and E'_q are the direct and quadrature axis voltages. X' is the transient reactance and X_o the rotor open-circuit reactance. T'_o is the rotor open-circuit time constant. s is the slip of the motor. H_m is the inertia constant of the machine. ω_b is the angular velocity of the stator field in rad/s. X_s is the stator reactance, and X_r is the rotor reactance. X_m is the magnetizing reactance. R_s is the stator resistance, and R_r is the rotor resistance. T_e is the developed electrical torque, and T_m is the per unit mechanical load torque. I_{sd} and I_{sq} are the d- and q-axis components of the stator current, respectively. V_{sd} and V_{sq} are the terminal direct and quadrature voltages in the d-q reference frame.

In order to introduce flexibility of the model, according to Khlifi et al,[35] the mechanical torque equation depends quadratically on the speed as given in Equation (6):

$$T_m = \mathrm{a} + \mathrm{b}\omega + \mathrm{c}\omega^2 + d\omega^{\alpha_m} \tag{9}$$

Here, ω is the angular velocity with respect to a synchronous reference.

α_m is the speed torque sensitivity coefficient.

a, b, c, and d are the model coefficients of the machine torque model satisfying the condition $c = 1 - (a+b+d)$.

Exponential recovery loads

The electrical heating loads constitute lighting, heating, and motors plus some levels of transformer tap changing. Power system voltage stability is significantly influenced by the massive amount of electrical heating loads. Karlsson and Hill[36] have studied critical effect of electrical heating loads on power system voltage stability and proposed a load model with exponential recovery.

Load restoration procedure is the dynamic behavior of various loads and controllers. This procedure restores load power to a certain level closed to its nominal value. Since loads draw more power during this procedure, voltage instability occurs. To self-restoring load, load state variable modeled with an exponential type of voltage characteristics is added to the transient behavior.

Active and reactive powers have a nonlinear dependency on voltage. A set of nonlinear equations represents the model. The dynamic model for the active power is given as,

$$\dot{x}_p = -\frac{x_p}{\mathrm{T}_p} + P_0\left(\left(\frac{v}{v_0}\right)^{x_s} - \left(\frac{v}{v_0}\right)^{xt}\right) \tag{10}$$

$$p = \frac{x_p}{\mathrm{T}_p} + P_0\left(\frac{v}{v_0}\right)^{x_t} \tag{11}$$

where

P	actual active consumed by the load;
P_0	nominal load power consumption;
v_0	reference voltage;
T_p	active power recovery time constants;
x_p, x_q	state variables of load dynamics;
α_s, α_t	steady-state and transient active power voltage dependency factors.

Similar equations hold for the reactive power Q also. The load behavior is thus characterized by a time constant T_q and transient and steady-state load-voltage dependence parameters β_t and β_s. T_p represents the time that the power recovery needs to reach 63% of its final value α_s, or the steady-state load-voltage dependence quantifies how much load has been restored after the recovery; a value equal to 0 means a fully restored load, while a value other than 0 indicates partly restored load. Furthermore, the parameter α_s representing steady-state voltage dependency may have negative values.

Due to system disturbance, there is drop in the voltage. This voltage drop starts the transient and the power drop instantaneously. As soon as power drop, the load state variable x_p and x_q start recovering the power to its nominal values.[37,38]

3 | SYSTEM DIFFERENTIAL-ALGEBRAIC MODEL

A set of differential algebraic equations is used to represent the overall distribution network incorporating synchronous generators, DFIG-based wind farm, transmission lines, transformers, composite loads, and other control devices/systems, as discussed above. The rest of the system is represented by an infinite bus. The DAE has the general form that belongs to a class of nonlinear systems, as follows:

$$\dot{x} = f(x, y, \lambda_w, \lambda_L) \tag{12a}$$

$$0 = g(x, y, \lambda_w, \lambda_L) \tag{12b}$$

The nonlinear function $\boldsymbol{f}$ is directly related with the state variable x, and signifying the system differential equations, such as the dynamic state variables of the DFIG wind turbine and its controls and of the composite load dynamics and system controllers. The nonlinear function $\boldsymbol{g}$ characterizes the system nonlinear algebraic constraints. It typically results from neglecting fast dynamics and comprises of the wind generator stator voltages/currents in the subvector (y_{stat}) and the network voltages/phase angles in the subvector (y_{net}). The vector x given above has three partitions. The first partition pertains to the wind generator model, the second motor load, and the third represents the exponential recovery load.

Since bifurcation theory is an outstanding tool of researching on voltage stability, it has been extensively applied in examining the power system voltage stability. For diverse characteristics of active components, such as wind power generation and changes in load parameters in power system, analysis methods of bifurcation are fragmented into single-parameter, two-parameter, and multiparameter according to the number of bifurcation control parameters. This paper presents a research study on voltage stability using two-parameter bifurcation analysis method.

The principle control parameter is the wind power generation λ_w; the other bifurcation parameter is the composite load parameter vector defined as,

$$\lambda_L = \left[\lambda_{zip} \;\; \lambda_{mot} \;\; \lambda_{rec}\right]^T \tag{13}$$

The motor load bifurcation parameter λ_{mot} is the vector of the motor torque model coefficients of the per unit component of mechanical motor torque T_m, λ_{mot} = [a, *b*, *c*, *d*] as given in Equation (9). λ_{mot} = *a*,*b*,*c*,*d*. The algebraic stator equations in (12a) to (14) express the voltage-current relationship. The network equations given below in (14) express the nodal power balance, among the generationP_{Gi}+jQ_{Gi}, the power consumption $P_{Li}(\theta, V, \lambda_L) = P_i^{ZIP} + P_i^{mot} + P_i^{rec}$, and injection, at each bus,

$$\begin{aligned} P_i - \left[P_{G_i} - \left(P_i^{ZIP} + P_i^{mot} + P_i^{rec}\right)\right] &= 0 \\ Q_i - \left[Q_{G_i} - \left(Q_i^{ZIP} + Q_i^{mot} + Q_i^{rec}\right)\right] &= 0. \end{aligned} \tag{14}$$

where $V_i \angle \theta_i$ is the nodal complex voltage of the *i*th bus. $\overline{Y}_{ij} = G_{ij} + jB_{ij}$ is the transfer admittance; $\overline{Y}_{Cij} = G_{Cij} + jB_{Cij}$ is the equivalent charging admittance and $\theta_{ij} = \theta_i - \theta_j$.

The system's equilibrium point constitutes the nominal points (x_0, y_0, λ_{L0}) satisfying Equations (12a) and (12b), can be written as

$$\begin{aligned} 0 &= f(x_0, y_0, \lambda_0) \\ 0 &= g(x_0, y_0, \lambda_0) \end{aligned} \tag{15}$$

Consequently, the equilibrium solution manifold can be inferred as

$$\lambda = \{(x, y, \lambda) / f(x, y, \lambda) = 0, g(x_0, y_0, \lambda_0) = 0\} \tag{16}$$

The x and y vectors have the form given below:

$$x = \left[E' \; \delta \; s^D \; i_{rd} \; i_{rq} \; \theta_p : E'_d \; E'_q \; s^m : x_p \; x_q\right]^T = \left[\left(X^D\right)^T \quad \left(X^m\right)^T \quad \left(X^R\right)^T\right]^T \tag{17}$$

$$y = \left[I_d^D \; I_q^D \; V_d^D \; V_q^D \; I_d^m \; I_q^m \; V_d^m \; V_q^m : \theta_{1\cdots n} \; V_{1\cdots n}\right]^{\hat{A}T} = \left[y_{stat}^T \; y_{net}^T\right]^T \tag{18}$$

For small signal stability analysis, the DAE set ((12a) and (12b)) is linearized at a steady-state operating point, yielding the system Jacobian matrix J_{sys} as defined in (19):

$$\begin{bmatrix} \Delta\dot{X}^D \\ \Delta\dot{X}^m \\ \Delta\dot{X}^{rec} \\ \cdots \\ 0 \\ 0 \end{bmatrix} = \begin{bmatrix} f_{DD} & f_{DM} & f_{DR} & \vdots & f_{D,y_{sta}} & f_{D,y_{net}} \\ f_{MD} & f_{MM} & f_{MR} & \vdots & f_{M,y_{sta}} & f_{M,y_{net}} \\ f_{RD} & f_{RM} & f_{RR} & \vdots & f_{R,y_{sta}} & f_{R,y_{net}} \\ \cdots & \cdots & \cdots & \vdots & \cdots & \cdots \\ g_{S_t,X^D} & g_{S_t,X^m} & g_{S_t,X^{rec}} & \vdots & g_{S_t,y_{sta}} & g_{S_t,y_{net}} \\ g_{P_Q,X^D} & g_{P_Q,X^m} & g_{P_Q,X^{rec}} & \vdots & g_{P_Q,y_{sta}} & g_{P_Q,y_{net}} \end{bmatrix} \begin{bmatrix} \Delta X^D \\ \Delta X^m \\ \Delta X^{rec} \\ \cdots \\ \Delta y_{sta} \\ \Delta y_{net} \end{bmatrix} \tag{19}$$

where f_{pq} is the Jacobian of the vector X^p with respect to the vector X^q; p and q take values D, m, R, θ, and V. Also, Δ designates a small increment in corresponding variables. The variables $g_{(.)}$ correspond to the algebraic equation. Let us define

$$g_y = \begin{bmatrix} g_{St,ysta} & g_{St,ynet} \\ g_{PQ,ysta} & g_{PQ,ynet} \end{bmatrix} \tag{20}$$

From Schurr's theorem,[38] if g_y is invertible, ie, nonsingular along a solution path of Equation (19)), an equivalent reduced dynamic system may be obtained as follows:

$$\Delta \dot{x} = \left(f_x - f_y g_y^{-1} g_x\right).\Delta x = Jred.\Delta x \tag{21}$$

Singularity-induced bifurcation (SIB) occurs in the system as soon as *det* (g_y) is equal to zero. For the dynamic bifurcation phenomenon, it is always assumed that *det* (g_y) is not equal to zero and that g_y^{-1} exists.[39] Dynamic voltage stability analysis is performed by analyzing the characteristic root of the system state's Jacobian matrix J_{red}.

Under the assumption of small deviations in the dynamic state variables, and in generator terminal voltage settings, the load flow model J_{LF} is obtained as

$$J_{LF}(\lambda_w, \lambda_L) = g_{P_Q y_{net}} = \begin{bmatrix} g_{P\theta} & g_{PV} \\ g_{Q\theta} & g_{QV} \end{bmatrix} \tag{22}$$

The first derivatives of the power mismatch Equation (14) with respect to voltage magnitudes and angles:

$$J_{LF}(\lambda_w, \lambda_L) = J^o - \left[J^{ZIP} + J^{rec}\right] \tag{23}$$

where$J^o$is the Jacobian matrix with constant power loading and $J^{ZIP}$and J^{rec} are the Jacobians associated with voltage dependent load components:

$$J^{\text{ZIP}} = \begin{bmatrix} 0 & \text{L} & 0 & J^{\text{ZIP}}_{\text{P}_1} & 0 & 0 \\ \text{M} & \text{O} & 0 & 0 & \text{O} & 0 \\ 0 & 0 & 0 & 0 & 0 & J^{\text{ZIP}}_{\text{P}_\text{N}} \\ 0 & \text{L} & 0 & J^{\text{ZIP}}_{\text{Q}_1} & 0 & 0 \\ \text{M} & \text{O} & \text{M} & 0 & \text{O} & 0 \\ 0 & 0 & 0 & 0 & 0 & J^{\text{ZIP}}_{\text{Q}_\text{N}} \end{bmatrix} J^{\text{rec}} = \begin{bmatrix} 0 & \text{L} & 0 & J^{\text{rec}}_{\text{P}_1} & 0 & 0 \\ \text{M} & \text{O} & 0 & 0 & \text{O} & 0 \\ 0 & 0 & 0 & 0 & 0 & J^{\text{rec}}_{\text{P}_\text{N}} \\ 0 & \text{L} & 0 & J^{\text{rec}}_{\text{Q}_1} & 0 & 0 \\ \text{M} & \text{O} & \text{M} & 0 & \text{O} & 0 \\ 0 & 0 & 0 & 0 & 0 & J^{\text{rec}}_{\text{P}_\text{N}} \end{bmatrix} \tag{24}$$

$$J^{ZIP}_{P_1} = \frac{P_{oi}}{V_{oi}}(2a_{1i} + a_{2i}),\ J^{ZIP}_{Q_1} = \frac{Q_{oi}}{V_{oi}}(2b_{1i} + b_{2i}),\ J^{rec}_{P_1} = \alpha^P_t \frac{P_{oi}}{V_{oi}} V_i^{\alpha^P_t - 1},\ J^{rec}_{Q_1} = \alpha^Q_t \frac{Q_{oi}}{V_{oi}} V_i^{\alpha^Q_t - 1} \tag{25}$$

4 | ANALYSIS OF CODIMENSION BIFURCATION

Bifurcation theory analyses the quantitative and qualitative information about the behavior of a nonlinear system close to bifurcation equilibrium points with changes in system parameters.[40] The parameters are assumed to change "slowly," so that the system can move from one equilibrium point to another equilibrium point with these changes. Therefore, bifurcation analysis is usually associated with the study of equilibria of the nonlinear system model.[41]

In power systems, SNBs and some types of limit-induced bifurcation (LIBs) are characterized by the local integration and loss of power flow solutions with gradual changes in certain system parameters, mostly system demand. This phenomenon has been associated with VS problems.[41] These kinds of bifurcations are also referred as "fold" or "turning points."

Locating the saddle-node and HBs by computational approaches comprise continuation and direct methods. The equilibrium conditions of the nonlinear system given in Equations (12a) and (12b) are obtained with the simplified expression of $f(x, \lambda) = 0$.

An approximate bifurcation point is attained with application of continuation method. Later, direct method is applied to obtain more precise single-parameter bifurcation point. Thus, information of the middle process during parameter fluctuation and precise solution of the bifurcation point are acquired. On the basis of the above foundation, tracking of two-parameter local bifurcation boundary turn into an easy task. To trace static bifurcation (here means the SNB points) that the equilibrium prevalence satisfies[42] (Equation 12a), it is assumed that single-parameter bifurcation points of Equations (26a) to (26c) have been attained in line of abovementioned belief.

SNBs occur when static voltage collapse or angle instability may occur. It leads to singularity of the reduced state matrix J_{red}. J_{red} has zero eigenvalue, with nonzero eigenvectors.[43] In practice, SNB occurs when two equilibrium points, typically one stable and one unstable, merge together and appear as the parameter λ. PV curves illustrated in Figure 4A,B with slow change in λ, where V_{Gi} and Q_{Gi} stand for a *i*th generator terminal voltage magnitude and reactive power, respectively.

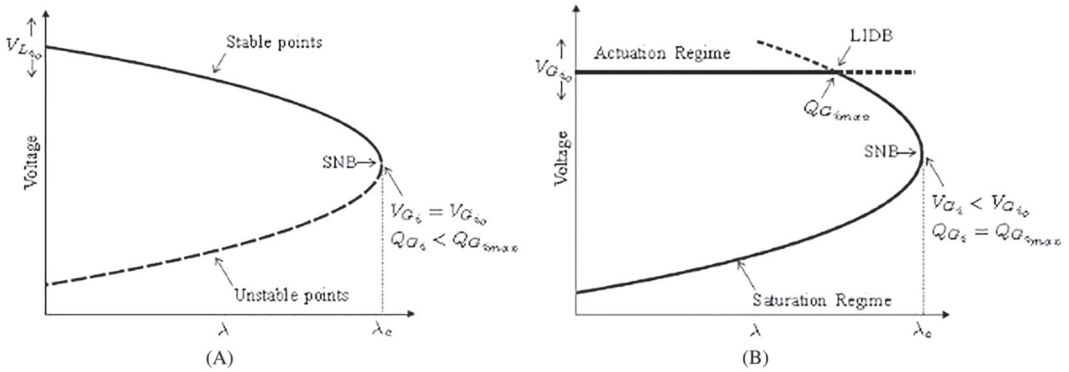

FIGURE 4 Main bifurcations observed in PV curves: (A) SNB without Q_G limits and (B) LIDB followed by an SNB

Mathematically, SNB is found by solving the set of equations,

$$F(x, y) = 0 \tag{26a}$$

$$F_x v = 0 \text{ or } w^T F = 0 \tag{26b}$$

$$\|v\| = 1 \text{ or} \|w\| = 1 \tag{26c}$$

where $v,w \in R^N$*where* $v,w \epsilon R^N$ is the right and left eigenvector of the Jacobian matrix. Equations (26a) and (26b) ensure the nontrivial condition for F at an equilibrium point defined by (12a). The problem is solved with Newtown-Raphson algorithm. The neighboring equilibrium point adjacent to the SNB point is obtained by solving Equation (27):

$$\begin{aligned} &F(x, y) = 0 \\ &(F_x - \varepsilon I)v = 0 \end{aligned} \tag{27}$$

where ε is a small real number,

I is the identity matrix of the same order as the Jacobian F_x.

It is evident that the bifurcation point is obtained with $\varepsilon = 0$.[44] Beyond this SNB point, these equations have no real solution. But it is determined through the continuation methods or the so-called direct methods. The basic idea of the proposed method is an extension of SNB point by one-parameter and continuation method. The nonlinear equations which express SNB point are solved and traced with the help of continuation method with two parameters resulting in tracing out two-dimensional bifurcation of the system.

HBs occur when J_{red} has a pair of conjugate eigenvalues crossing the imaginary axis while the other eigenvalues have negative real parts, and an unstable oscillatory behavior may occur.[25] It is desirable to design compensator to ensure a sufficiently large margin to HB. The margin is often expressed in a parameter space that includes load powers and controllable or tunable parameters. The margin is measured assuming a direction of load increase with continuation software.

HB can be computed by solving the equations given below.

$$\begin{aligned} &F(x, y) = 0 \\ &\|v\| = 1 \\ &J_s^T(x, y)v' + wv'' = 0 \\ &J_s^T T(x, y)v'' + wv' = 0 \end{aligned} \tag{28}$$

where the system Jacobian J_s^T is the reduced form of $J_s^T = f(f_x - f_y g_y^{-1} g_x)$,

where $0 \pm jw$ are the eigenvalues corresponding to the HB, and $v = v' \pm jv''$ are the corresponding left side eigenvectors. The last equation is the nontrivial condition. It is solved with Newton Raphson optimization method. These two approaches belong to the direct method. With respect to two-parameter bifurcation analysis of HB, based on continuation method, only tracking of two-dimensional bifurcation boundary in power systems has been reported.[45]

In Slimene and Khlifi,[46] two-parameter bifurcation analysis has been conducted on a typical power system model. The SNB curve and HB curve have been obtained in parameter space considering active and reactive load effect on voltage stability. Iterative Newton expansion equation has

been proposed to solve HB in Li.[47] This method not only avoids the SNB system Jacobian matrix at the vicinity of bifurcation point singularity but also overcomes difficulty of selecting initial value, and the computing speed was improved.

Two-parameter bifurcation analysis of power systems is mainly based on SNB and HB, so other types of bifurcation and its two-parameter bifurcation analysis are severely needed. Although the research on two-parameter bifurcation analysis is still in its infancy stage, the importance of two-parameter bifurcation analysis is not in doubt.

Studies showed that in comparison with single parameter, analysis of multiparameter bifurcation reveals further significant effects of system parameters to the power system voltage stability.

5 | ASSESSMENT METHODOLOGY

The study is based on defining four system models by combining the wind DFIGs with different load models: static ZIP, exponential recovery, induction motor, and composite load model. The model parameters and variables are given in Table 1. The stability of an equilibrium point and associated local bifurcations are determined from the eigenvalues of the reduced system matrix J_{red} mentioned in (Equation 21).

Standard PV curves are based on CPF algorithms applied to the combined system of algebraic and differential equations. The DAEs are solved using a pseudoarclength continuation strategy[48] allowing detection of limit points and bifurcation points as functions of a system parameter. A scalar coefficient λ_G is used as a bifurcation parameter for wind power increase with respect to nominal power, $P_w = \lambda_G P_{w0}$. For the slack bus, which is assumed to be the high voltage feeder, its generation is not multiplied by λ_G, and thus, it can reverse its flow for high wind power penetration. The DFIGs are modeled as PV generator buses operated in voltage-controlled mode, with a power factor of about 0.95. The simulation tool is the Power System Analysis Toolbox (PSAT).[30] The original continuation power flow program has been modified to incorporate the wind power rather than the loading factor, as a bifurcation parameter.

A bifurcation diagram illustrates the long-term qualitative (periodic orbits or fixed points/equilibria) changes of a system as a function of system bifurcation parameter. A bifurcation diagram illustrates the complete dynamics of the system with the parameter variation. Wind power generation (λ_G) and loading factor (λ_L) are taken as bifurcation parameters to study the complete dynamics of the system.

Figure 5 demonstrates the bifurcation analysis procedure using PSAT. The primary task of acquiring codimension-two bifurcation points is to find the one-dimensional equilibrium solution iteratively. The iterative equilibrium solution can be expressed as in Equation (16).

Equation (16) is the curve defined by an n-dimensional variable $\boldsymbol{x}$ in $(n + 1)$-dimensional space. The iterative equilibrium solution is calculated using the continuation algorithm, ie, a series of points (x^i, λ^i), $i(1,2,3, \ldots.)$ along the direction of parameter variation are acquired through prediction and calibration from an initial point (x^0, λ^0). The normal equation is parameterized, and the bifurcation points are attained through prediction, calibration, and step-size tuning.

6 | SIMULATION RESULTS

The study model is a five-bus, 30-kV distribution network consisting of a wind farm injecting power via a 0.69/30-kV step-up transformer, then connected to a common load bus 3, via a transmission line of ratio X/R $\approx$ 1.5 as shown in Figure 6. The wind farm comprises of 25 × 2 MW DFIGs represented at their common connection point by a single equivalent turbine, assuming uniform wind speed distribution and identical electrical characteristics of all aggregated turbines.[49] Step-up transformers and collector system lines are aggregated as lumped parameters shown in Figure 6. The system parameters of the DFIG are given in Appendix A. The distribution network is connected to a high-voltage feeder via an LTC, and a capacitor is installed at bus 4 to help the voltage control. The base load power is P_{Lo} = 50 MWwith a power factor of 0.833. This choice is made so that the different load types are comparable in steady-state base consumption. Accordingly, the motor load consists of three parallel

TABLE 1 Proposed study cases

Model	Load Model	State Space Vectors	Bifurcation Parameters	
			Principle	Other Parameters
1	ZIP	$x = [E', \delta, s^D, i_{rd}, i_{rq}, \theta_p]^T$, $y = \left[I_d^D, I_q^D, V_d^D, V_q^D, \theta_{1\cdots n}, V_{1\cdots n}\right]^T$	$\lambda_L = \lambda_{zip}$	λ_w
2	Exponential recovery	$x = [E', \delta, s^D, i_{rd}, i_{rq}, \theta_p, x_p, x_q]^T$, $y = \left[I_d^D, I_q^D, V_d^D, V_q^D, \theta_{1\cdots n}, V_{1\cdots n}\right]^T$	$\lambda_L = \lambda_{rec}$	λ_w
3	Induction motor	$x = \left[E', \delta, s^D, i_{rd}, i_{rq}, \theta_p, E_d', E_q', s^m\right]^T$, $y = \left[I_d^D, I_q^D, V_d^D, V_q^D, I_d^m, I_q^m, V_d^m, V_q^m, \theta_{1\cdots n}, V_{1\cdots n}\right]^T$	$\lambda_L = \lambda_{mot}$ a,b,c	λ_w
4	Composite load	$x = \left[E', \delta, s^D, i_{rd}, i_{rq}, \theta_p, E_d', E_q', s^m, x_p, x_q\right]^T$ $y = \left[I_d^D, I_q^D, V_d^D, V_q^D, I_d^m, I_q^m, V_d^m, V_q^m, \theta_{1\cdots n}, V_{1\cdots n}\right]^T$	$\lambda_L = \lambda_{zip}+\lambda_{rec}+\lambda_{mot}$	λ_w

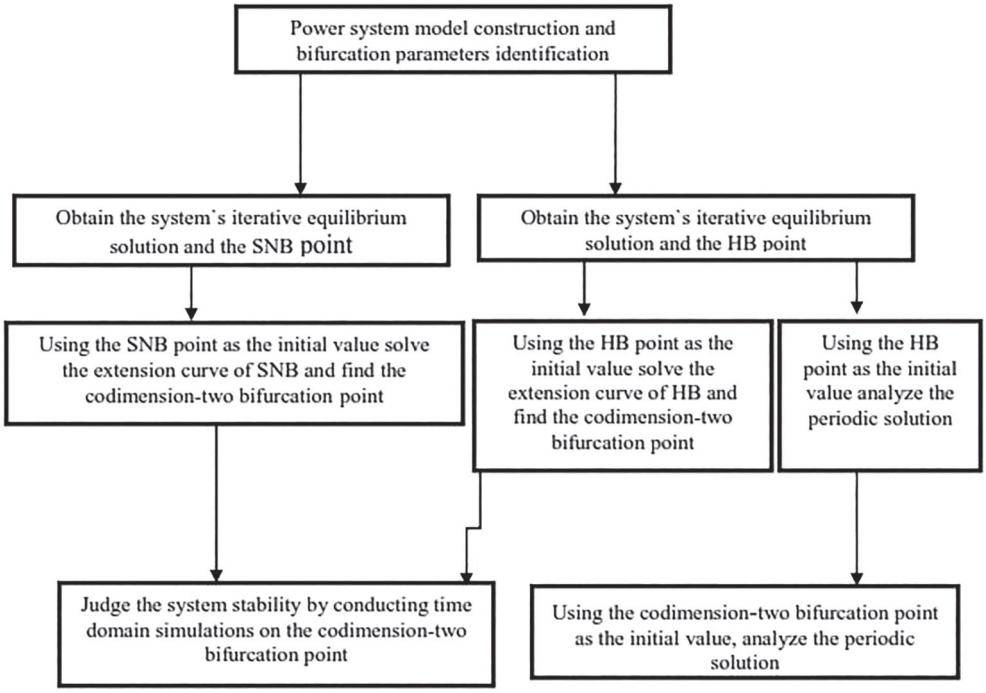

FIGURE 5 Flow chart of the bifurcation method using Power System Analysis Toolbox (PSAT)

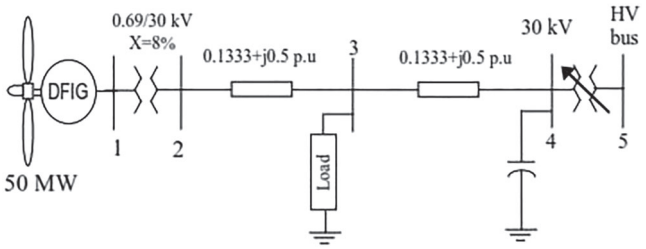

FIGURE 6 Test power system

motors of 20 MVA rating each, with 0.833 power factor. Initial steady-state operation with reduced wind power generation (P_w = 0.01 pu) is simulated and given in Table 2. It is noted that the load is supplied via the distribution feeder from the infinite bus. Voltages are maintained at the DFIG and slack buses. At the PQ buses, the voltages remain at slightly lower values and slightly higher values at the LTC secondary bus.

6.1 | Static load model

Loading margin for various static load types (model 1 in Table 1), chosen to demonstrate the differences in static analysis, for a steady-state wind generation of 50 MW at 0.95 power factor as shown in Figure 7A. The industrial motor load exhibits lowest voltage profile and considerably smaller loading margin. Highest voltage profile and loading margins are observed for the water heater load followed by the commercial load. It is because water heater is having highest power factor resulting in no reactive power. On the other hand, large industrial motor exhibits lowest power factor due to which it draws large reactive power. So reactive power is having close association with low margin; the larger the reactive

TABLE 2 System initial state with low wind power generation

Bus	Bus 1	Bus 2	Bus 3	Bus 4	Bus 5
LF model	PV	PQ	PQ	PQ	Slack
V (pu)	1.0	0.9990	0.9822	1.0129	1.0
P_G (pu)	0.01	0	0	0	0.3029
Q_G (pu)	0.0120	0	0	0	−0.0491

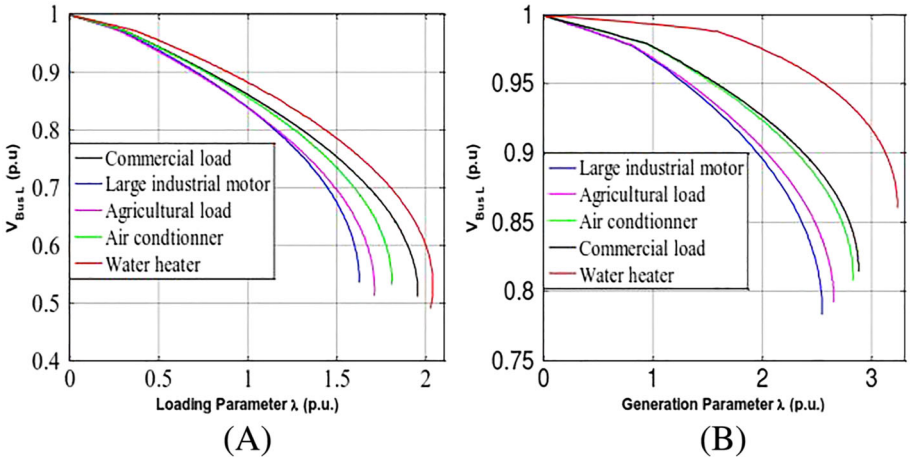

FIGURE 7 Load bus voltage function of (A) load increase and (B) wind generation margins for different static load models [Colour figure can be viewed at wileyonlinelibrary.com]

power, the smaller the loading margin. Likewise, we tested the wind generation margins for different load types with fixed load parameters. The bifurcation diagrams show different collapse points for the different loads as shown in Figure 7B. The water heater load exhibited the highest voltage profile and highest wind generation margin of about 3.5 pu, followed by the commercial load. The large industrial motor allowed only 2.6 pu wind power generation margin. The explanation is the same as above.

Two-parameter bifurcation diagrams are then obtained in Figure 8A,B, for the two extreme cases of water heater load and large industrial motor load. We have chosen these two cases because they represent the limiting cases as is demonstrated in Figure 3A,B.

Figure 9A shows bifurcation lines in two-parameter space for water heater load. The line for SNB is shown in red, LIB (I) in blue, and LIB (Q_G) in green. From the figure, the SNB for the values λ_G: [0 → 0.5] λ_L is increasing from 1.8 pu to its maximum value $\lambda_{L,max}$ = 2.05 pu at λ_G = 0.5 pu, and for λ_G: [0.5 → 2.4], λ_L is drooping to its minimum value $\lambda_{L,min}$ = 0.5 pu at λ_G = 2.4 pu. The LIB (I) for the values λ_G: [0 → 1.0] λ_L is increasing from 1.25 pu to its maximum value $\lambda_{L,max}$ = 1.6 pu at λ_G = 1.0 pu, and for λ_G: [1.0 → 2.4], λ_L is decreasing to its minimum value $\lambda_{L,min}$ = 0.5 pu at λ_G = 2.4 pu. The LIB (Q_G) for the values λ_G: [0 → 1.5] λ_L is increasing from 0.05 pu to its maximum value $\lambda_{L,max}$ = 0.6 pu at λ_G = 1.5 pu, and for λ_G: [1.5 → 2.4], λ_L is decreasing to its minimum value $\lambda_{L,min}$ = 0.05 pu at λ_G = 2.4 pu.

Figure 9B shows bifurcation lines in two-parameter space for large industrial motor load. The lines for SNB are shown in red, LIB (I) in blue, and LIB (Q_G) in green. From the figure, the SNB for the values λ_G: [0 → 0.5] λ_L is increasing from 1.5 pu to its maximum value $\lambda_{L,max}$ = 1.7 pu at λ_G = 0.5 pu., and for λ_G: [0.5 → 2.4], λ_L is drooping to its minimum value $\lambda_{L,min}$ = 0.5 pu at λ_G = 2.4 pu. The LIB (I) for the values λ_G: [0 → 1.0] λ_L is increasing from 1.05 pu to its maximum value $\lambda_{L,max}$ = 1.3 pu at λ_G = 1.0 pu, and for λ_G: [1.0 → 2.4], λ_L is decreasing to its minimum value $\lambda_{L,min}$ = 0.5 pu at λ_G = 2.4 pu. The LIB (Q_G) for the values λ_G: [0 → 0.25] λ_L is constant at 0.1 pu, for λ_G: [0.25 → 1.0], λ_L is increasing from 0.1 pu to its maximum value $\lambda_{L,max}$ = 0.4 pu at λ_G = 1.0 pu; again, for the values λ_G: [1 → 1.5], λ_L is constant at 0.4 pu, and for λ_G: [1.5 → 2.4], λ_L is decreasing to its minimum value $\lambda_{L,min}$ = 0.05 pu at λ_G = 2.4 pu.

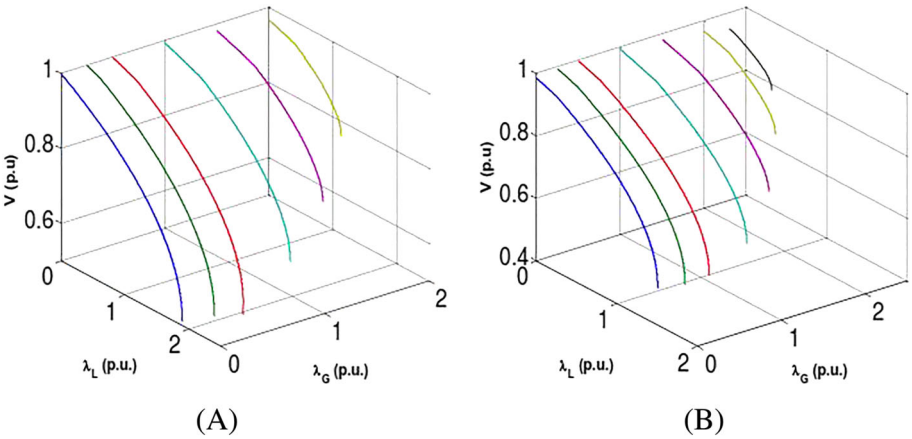

FIGURE 8 Two-parameter bifurcation for load bus voltage; the principle bifurcation parameter is the loading margin. A, Case of water heater load. B, Case of large industrial motor load [Colour figure can be viewed at wileyonlinelibrary.com]

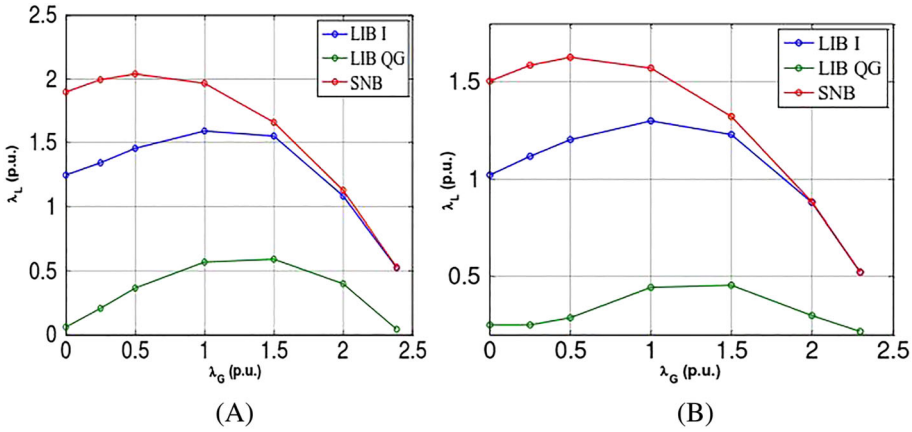

FIGURE 9 Bifurcation lines in two parameter space. A, Case of water heater load. B, Case of large industrial motor load [Colour figure can be viewed at wileyonlinelibrary.com]

The continuation of the SNB curve highlights that for small values of λ_G (less than 0.5 pu), the SNB point occurs at highest loading level values. On the other hand, for wind generation levels over 2.0 pu, the SNB point occurs at smaller loading.

From the above analysis for SNB and LIB (I), first the increase in loading margin and then the decrease with respect to the incremental increase in the generation margin are because of the thermal limit of the cable transmission line. For LIB (Q_G) with an incremental increase in λ_G, the loading margin increases to its maximum value and then decreases. This increase in loading margin is due to reactive power supplied by the DFIG, and the decrease in loading margin is because DFIG has reached its saturation limit of supplying maximum reactive power.

6.2 | Dynamic load model

6.2.1 | Exponential recovery load

For the exponential recovery load model, the coefficients are from Leung and Hill.[37] PV curve method is used to analyze the effect of power generation margin on bifurcation points. A two-dimensional bifurcation analysis is performed. Summation of the active power *P*1 and reactive power *Q*1of the exponential recovery load is taken as the loading parameter λ_L, while the generation margin λ_G is taken as the second parameter for bifurcation control.

Two parameter bifurcation diagrams are then obtained for the different possible values of λ_L and λ_G for thermostatic controlled load and shown in Figure 10A. Figure 10B depicts bifurcation lines in two-parameter space for exponential recovery load. The line for SNB is shown in red, LIB (I) in blue, and LIB (Q_G) in green.

From the figure, the SNB for the values λ_G: [0 → 0.5] λ_L is increasing from 1.45 pu to its maximum value $\lambda_{L,max}$ = 1.6 pu at λ_G = 0.5 pu; for λ_G: [0.5 → 1.5], λ_L is decreasing up to λ_L = 1.3 pu at λ_G = 1.5 pu, and for λ_G: [1.5 → 2.1], λ_L is drooping to its minimum value $\lambda_{L,min}$ = 0.7 pu at λ_G = 2.1 pu. The LIB (I) for the values λ_G: [0 → 0.5] λ_L is increasing from 1.1 pu to its maximum value $\lambda_{L,max}$ = 1.25 pu at λ_G = 0.5 pu; for λ_G: [0.5 → 1.5], λ_L remains unchanged at λ_L = 1.25 pu, and for λ_G: [1.5 → 2.1], λ_L is drooping to its minimum value $\lambda_{L,min}$ = 0.65 pu at λ_G = 2.1 pu. The LIB (Q_G) for the

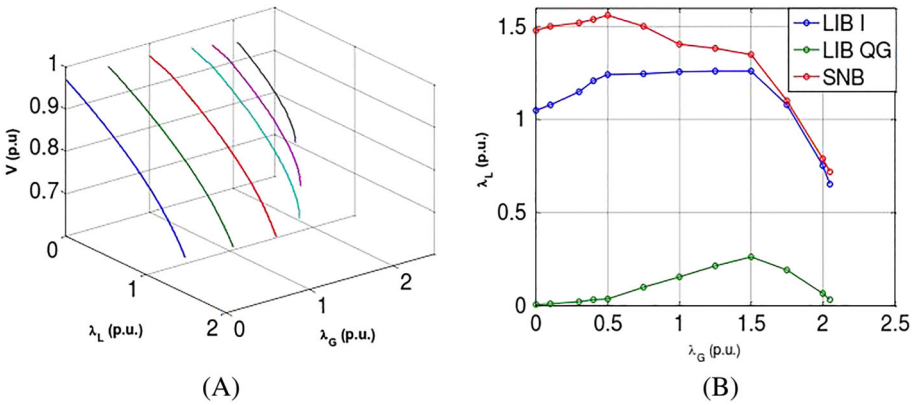

FIGURE 10 Two-parameter bifurcation (A) and bifurcation lines (B) in two-parameter space [Colour figure can be viewed at wileyonlinelibrary.com]

values λ_G: [0 → 0.5] λ_L is increasing slowly from 0.00 pu to its a value λ_L = 0.1 pu at λ_G = 0.5 pu; for λ_G: [0.5 → 1.5], λ_L further increased up to its maximum value $\lambda_{L,max}$ = 0.25 pu at λ_G = 1.5 pu, and for λ_G: [1.5 → 2.1], λ_L is drooping to its minimum value $\lambda_{L,min}$ = 0.05 pu at $\lambda_{::G}$ = 2.1 pu. The continuation of the SN bifurcation curve highlights that for small values of P_w (less than 0.7 pu), the SN bifurcation point occurs at higher loading level values. On the other hand, for wind generation levels over 0.8 pu, the SN bifurcation point occurs at smaller loading.

6.2.2 | Induction motor

Three dynamic motor loads are simulated for induction motor: Motor 1 has a constant torque load; motor 2 has a mechanical load with a strong linear dependence on speed, and motor 3 has a load with a strong quadratic dependence on speed:

Motor 1: $T_{L,1} = 0.3$ (pu)
Motor 2: $T_{L,2} = 0.07 + 0.16\omega + 0.07\omega^2$ (pu)
Motor 3: $T_{L,3} = 0.05 + 0.08\omega + 0.18\omega^2$ (pu)

The parameter values of these three induction motor loads are taken from Lerm and Canizares.[23] The dynamic interactions between each motor load type and the DFIG wind farm are tested by the bifurcation diagrams.

Two-parameter bifurcation surface (Figure 11) is shown for the different possible values of λ_L and λ_G for load of induction motor 1. Figure 12A to 12C is showing bifurcation lines in two-parameter space for loads on induction motor 1, motor 2, and motor 3, respectively. For all these cases, LIB (I) have not been detected. HB is observed only for loads on induction motor 1. The line for SNB is shown in red, LIB (Q_G) in green, and HB in blue.

From Figure 12A, the SNB for IM1 λ_L is increasing from 1.35 pu to its maximum value $\lambda_{L,max}$ = 1.45 pu at λ_G = 0.5 pu and remains constant up to at λ_G = 1.0 pu with λ_G: [0 → 1.0]. λ_L is drooping to its minimum value $\lambda_{L,min}$ = 0.5 pu at λ_G = 2.3 pu with λ_G: [1.0 → 2.3]. The LIB (Q_G) λ_L remains constant λ_L = 0.15 pu for the values λ_G: [0 → 0.5]; then, λ_L is increasing up to its maximum value $\lambda_{L,max}$ = 0.40 pu at λ_G = 1.4 pu and droops down to its minimum value $\lambda_{L,min}$ = 0.00 pu at λ_G = 2.1 pu and remains at this value up to λ_G = 2.3 pu. The HB for IM1 λ_L is increasing from 1.35 pu and reaching its maximum value $\lambda_{L,max}$ = 1.45 pu at λ_G = 0.6 pu with λ_G: [0 → 0.6]. Further, λ_L is drooping to its minimum value $\lambda_{L,min}$ = 1.05 pu at λ_G = 1.4 pu with λ_G: [0.6 → 1.4].

From Figure 12B, the SNB for IM2 λ_L is increasing from 1.25 pu to its maximum value $\lambda_{L,max}$ = 1.3 pu at λ_G = 0.5 pu and remains unchanged up to at λ_G = 1.0 pu with λ_G: [0 → 1.0]. Further, λ_L is drooping to a value λ_L = 0.9 pu at λ_G = 2.0 pu with a sudden drop to its minimum value $\lambda_{L,min}$ = 0.5 pu at λ_G = 2.05 pu with λ_G: [1.0 → 2.05]. The LIB (Q_G) λ_L remains constant λ_L = 0.15 pu for the values λ_G: [0 → 0.5]; then, λ_L is increasing up to its maximum value $\lambda_{L,max}$ = 0.325 pu at λ_G = 1.0 pu and remains unchanged up to λ_G = 1.5 pu with λ_G: [0.5 → 1.5]. Further, it decreases to its minimum value $\lambda_{L,min}$ = 0.05 pu at λ_G = 2.05 pu with λ_G: [1.5 → 2.05].

From Figure 12C, the SNB for IM3 λ_L is increasing from 1.35 pu to its maximum value $\lambda_{L,max}$ = 1.45 pu at λ_G = 0.5 pu and remains unchanged up to λ_G = 1.0 pu with λ_G: [0 → 1.0]. Further, λ_L is drooping to its minimum value $\lambda_{L,min}$ = 0.5 pu at λ_G = 2.3 pu with λ_G: [1.0 → 2.3]. The LIB (Q_G) λ_L remains constant λ_L = 0.15 pu for the values λ_G: [0 → 0.5]; then, λ_L is increasing up to its maximum value $\lambda_{L,max}$ = 0.40 pu at λ_G = 1.0 pu and remains constant up to λ_G = 1.5 pu with λ_G: [0.5 → 1.5]. Further, its droops down to its minimum value $\lambda_{L,min}$ = 0.01 pu at λ_G = 2.1 pu and remains at this value up to λ_G = 2.3 pu.

For LIB (Q_G), loading margin remains constant during initial increase in λ_G. It is because all active and reactive power generated by DFIG is injected to IM (all cases IM). Further increase in λ_G first increases loading margin and then decreases. This decrease is because of saturation of reactive power limit of DFIG. Further increase in λ_G results a constant value of loading margin; it is attributed to functioning of DFIG as load bus. The continuation of the SN bifurcation curve highlights that for small values of P_w (less than 1.1 pu) for IM1 and IM2 and less than 0.8 pu for IM3, the SN bifurcation point occurs at higher loading level values. On the other hand, for wind generation levels over 2.0 pu for IM1 and IM2 and over 0.8 pu for IM3, the SN bifurcation point occurs at smaller loading.

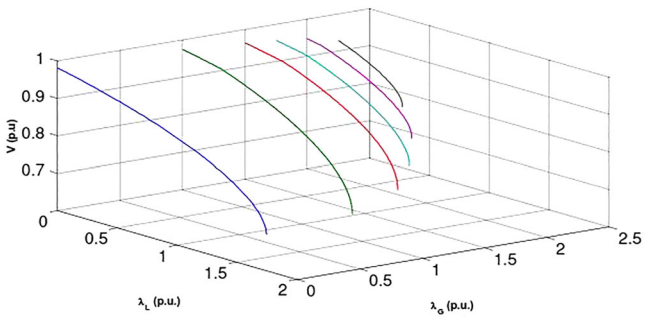

FIGURE 11 Two-parameter bifurcation for load bus voltage; the principle bifurcation parameter is the loading margin induction motor load 1 [Colour figure can be viewed at wileyonlinelibrary.com]

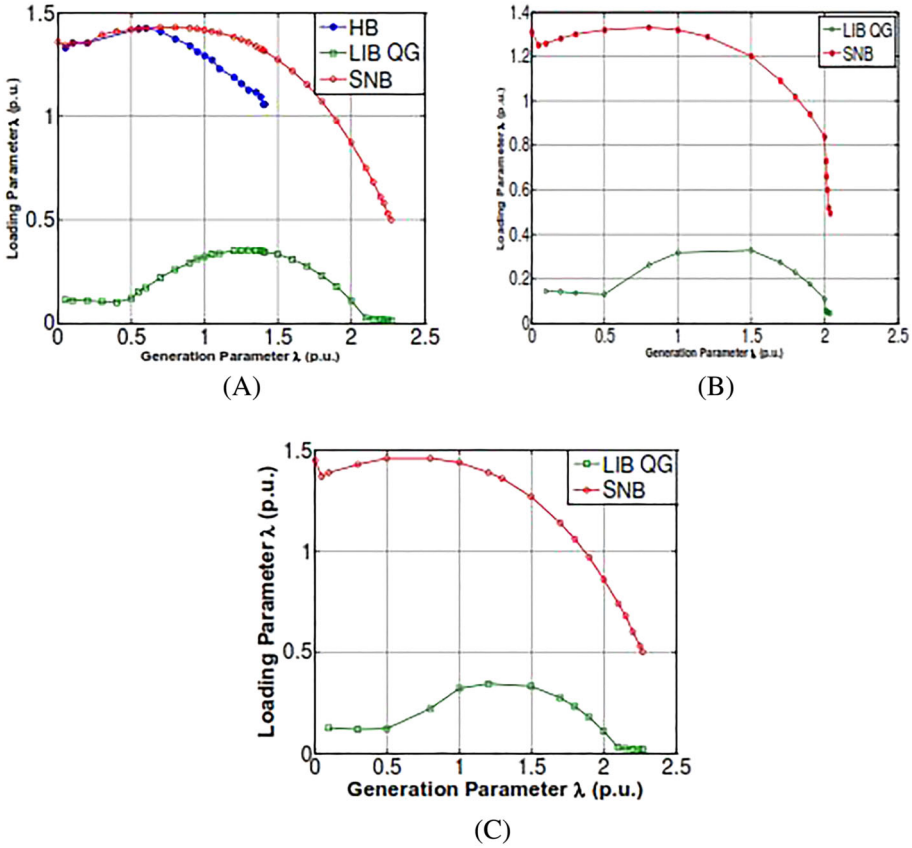

FIGURE 12 Bifurcation lines in two parameter space: (A) case of IM1, (B) case of IM2, and (C) case of IM3 [Colour figure can be viewed at wileyonlinelibrary.com]

There is no occurrence of HB with the IM2 and IM3 models. IM1 load models, which is constant stresses the system the most. Since IM2 model has mechanical load with a strong linear dependence on speed and IM3 has a load with a strong quadratic dependence on speed, IM2 and IM3 models are the least demanding one. These results are consistent with what is available in the literature related to power system stability.

6.2.3 | Composite load model

Two-parameter bifurcation surface (Figure 13A) is shown for the different possible values of λ_L and λ_G for composite load. Figure 13B is showing bifurcation lines in two-parameter space for composite load. HB is also observed for composite load. The line for SNB is shown in red, LIB (Q_G) in green, and HB in blue.

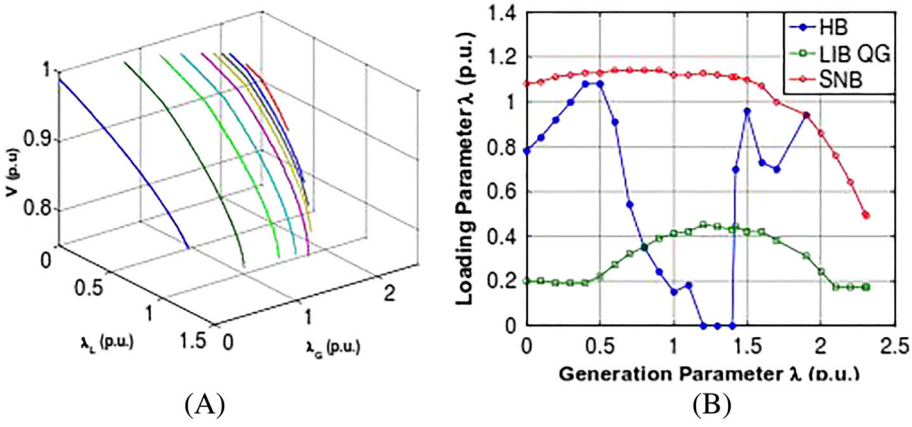

FIGURE 13 Two-parameter bifurcation and bifurcation lines in two parameter space. Case of composite load [Colour figure can be viewed at wileyonlinelibrary.com]

From Figure 13B, the SNB for composite load λ_L remains constant with its maximum value $\lambda_{L,max}$ = 1.1 pu for λ_G: [0 → 1.5]. λ_L is drops to its minimum value $\lambda_{L,min}$ = 0.3 pu at λ_G = 2.3 pu with λ_G: [1.5 → 2.3]. The LIB (Q_G) λ_L remains constant λ_L = 0.2 pu for the values λ_G: [0 → 0.5]; then, λ_L is increasing up to its maximum value $\lambda_{L,max}$ = 0.41 pu at λ_G = 1.4 pu and drops down to its minimum value $\lambda_{L,min}$ = 0.18 pu at λ_G = 2.1 pu and remains at this value up to λ_G = 2.3 pu for the values λ_G: [0.5 → 2.3].

The introduction of IM1 in composite load model, an oscillatory behavior is observed. Varying λ_G and λ_L simultaneously, HB points are identified. When λ_L is increasing from 0.8 pu and reaching its maximum value, $\lambda_{L,max}$ = 1.1 pu at λ_G = 0.5 pu with λ_G: [0 → 0.5]. λ_L is drooping to its minimum value $\lambda_{L,min}$ = 0.00 pu at λ_G = 1.2 pu with λ_G: [0.5 → 1.2]. Further, λ_L varies between these two limits for λ_G: [1.2 → 1.9].

The loading margin for composite load model with LIB (Q_G) and SNB is the same as explained in a static load case. But with HB in the first portion of increase in λ_G, loading margin is increasing and then decreasing to 0; it is because of the presence of IM. In the second portion, further increase in λ_G results in recovery in the loading margin which is attributed to the presence of exponential recovery load, because this load regulates its active and reactive power by adjustment of its parameters. The continuation of the SN bifurcation curve highlights that for small values of P_w (less than 1.6 pu), the SN bifurcation point occurs at higher loading level values. On the other hand, for wind generation levels over 2.0 pu, the SN bifurcation point occurs at smaller loading.

7 | CONCLUSION

A comparative stability analysis for a five-bus system based on two-parameter bifurcation, wind power generation, and loading margin has been studied using bifurcation diagram of variable speed wind turbine based on DFIG and various types of loads. It is established that assessment of maximal wind generation margin in the system highly depends on information about correct load models. It also concludes that power system small-signal stability and safety may be maintained by the values of occurrence of bifurcation points. It is evident from the experiment that connecting thermostatic controlled load provides the opportunities to maximize the generation margin stability of the power system. Moreover, most critical load for the generation margin stability of the wind power system has been influenced by the mechanical load of the induction motor which has a strong linear dependence on speed. The nature of the load shifts the location of the bifurcation points in the bifurcation diagram. The maximum deliverable power generation margin is determined by the location of the bifurcation points. Thus, maximum deliverable power generation margin is controlled by the nature of the load.

ORCID

Mohamed Arbi Khlifi https://orcid.org/0000-0003-2668-6533

REFERENCES

1. Mullane A, Lightbody G, Yacamini R. Wind-turbine fault ride-through enhancement. *IEEE Trans Power Syst*. 2005;20(4):1929-1937.
2. Shafiu, A., Bopp, T., Chilvers, I., Strbac, G., Active management and protection of distribution networks with distributed generation. In: Proc of IEEE PES General Meeting Denver, Jun 2004.
3. Western Electricity Coordinating Council Modeling and Validation Work Group, Composite load model for dynamic simulations, Report 1.0, June 12, 2012.
4. Wang Shu, Baran M. E, Reliability assessment of power systems with wind power generation, Conference: Power and Energy Society General Meeting, 2010 IEEE.
5. DOE-EPSA. Principles for increasing the accessibility and transparency of power system planning, Report, January 2017.
6. NERC. Distributed energy resources, connection modeling and reliability considerations, Task Force Report, February 2017.
7. Khlifi MA. Explaining the d-q magnetic couplings in saturated smooth air-gap ac machines. *Eng Technol Appl Sci Res*. 2019;9(1).
8. Gu Cheng-Hong, Ai Qian, Wu Jiayi, Department of Electrical Engineering, Shanghai Jiao Tong University, China. A study of effect of different static load models and system operating constrains on static voltage stability, Int. Conf. on Systems Theory and Scientific Computation, Malta, September 2005.
9. Zeng Zhiyuan, Li Xianqi, Zhou Jianzhong, Zhang Yongchuan. Investigation of wind farm on power system voltage stability based on bifurcation theory, Power and Energy Engineering Conference, 2009. APPEEC 2009. Asia-Pacific
10. Linh Nguyen Tung, Chuong Trinh Trong. Voltage stability analysis of grids connected wind generators, International Conference on Industrial Electronics and Applications, 2009.
11. Saïdi A, Ben Kilani K, Bouchoucha C, Elleuch M. Voltage regulation and dynamic performance of the tunisian power system with wind power penetration. *Trends Appl Sci Res*. 2011. ISSN 1819–3579;6(8):813-831. https://doi.org/10.3923/tasr.2011 © 2011 Academic Journals Inc
12. Toma Radu, Gavrilaș Mihai, Asachi Gheorghe. Voltage stability assessment for wind farms integration in electricity grids with and without consideration of voltage dependent loads. International Conference and Exposition on Electrical and Power Engineering (EPE 2016), 20–22 October, Iasi, Romania.
13. Dahal S., Mithulananthan N., Saha T.. Impact of composite loads on dynamic loadability of emerging distribution systems. Universities Power Engineering Conference (AUPEC), 2011 21st Australasian.
14. Khlifi MA. Analysis of an off-grid self-excited dual wound asynchronous generator for wind power generation. *Int J Adv Appl Sci*. 2019;6(6):35-42.

15. Muñoz J. C., and Cañizares C. A., Comparative stability analysis of DFIG-based wind farms and conventional synchronous generators, IEEE PES Power Systems Conference and Exposition, 2011.
16. Abdelaziz Saïdi, Khadija Ben Kilani and Elleuch Mohamed. Bifurcation in power systems distribution networks integrating variable speed wind generation. 6th IEEE International Multi-Conference on Systems, Signals and Devices, 2009.
17. Abdelaziz Saïdi, Khadija Ben Kilani and Elleuch Mohamed. Assessment of wind power penetration level in distribution network with consideration of static, motor and composite loads. The 5th IEEE International Renewable Energy Congress (IREC) March 25–27, 2014 in Hammamet – Tunisia.
18. Youjie M, Jidong Z, Xuesong Z, Wang XZ. Study on steady state voltage stability of power system containing wind farm based on bifurcation theory. *Power Syst Technol*. 2008;32(9):74-79.
19. Shaofeng Liu，Jinfeng Gao，Peng Li. Multi-parameter bifurcation analysis of excitation system with the Walve aggregated load model. *Proc CSEE*, 24 (12): pp 58–62, 2004.
20. Xiao K, Guo YJ, Tang Y, Haohui L. Two-parameter bifurcation analysis on a typical power system model. *Automation Electr Power Syst*. 2000;24(6):1-6.
21. Liu SF, Gao JF. Multi-parameter bifurcation analysis of excitation system with the Walve aggregated load model. *Proc CSEE*. 2004;24(12):58-62.
22. Dobson I, Lu L. New methods for computing a closest saddle node bifurcation and worst case load power margin for voltage collapse. *IEEE Trans PWRS*. 2015;8(3):240-243.
23. Lerm AAP, Canizares CA. Multi-parameter bifurcation analysis of the south Brazilian power system. *IEEE Trans on Power Syst*. 2003;18(2):737-846.
24. Ma YJ, Zhang JD, Zhou XS, Wang ZX. Study on steady state voltage stability of power system containing wind farm based on bifurcation theory. *Power Syst Technol*. 2008;32(9):74-79.
25. Li J, Zhou XS, Ma YJ. Multi-parameter Hopf bifurcation analysis of wind power system. *Power Syst Technol*. 2012;36(11):53-57.
26. Jiang P, Gu W, Tang GQ. Research on dynamic load margin of multi-machine power systems based on multi-parameter bifurcation analysis. *Trans China Electrotech Soc*. 2007;22(3):107-114.
27. Renmu H, Ma J, Hill DJ. Composite load modeling via measurement approach. *Power Syst IEEE Trans Power Syst*. 2006;21(2):663-672, May.
28. Feijóo A, Cidrás J, Carillo C. A third order model for the doubly-fed induction machine. *Electr Power Syst Res*. 2000;56(2):121-127, March.
29. Saidi A, Helmy W. Artificial neural network–aided technique for low voltage ride-through wind turbines for controlling the dynamic behavior under different load conditions. *Wind Eng J*, August 3. 2018. https://doi.org/10.1177/0309524X18791387
30. Milano F., PSAT, Matlab-based Power System Analysis Toolbox, Documentation for PSAT version 2.0.0, February 14, 2008, [Online]. Available: http://www.power.uwaterloo.ca/~fmilano/.
31. Bokhari A, Alkan A, Dogan R, et al. Experimental determination of the ZIP coefficients for modern residential, commercial, And Industrial Loads. *IEEE TRANS POWER DELIV*. JUNE 2014;29(3):1372-1381.
32. Kundur P. *Power machine stability and manipulate*. McGraw-Hill Inc; 1994.
33. IEEE challenge pressure on load representation for dynamic overall performance. General load fashions for energy go with the flow and dynamic performance simulation. *IEEE Trans Energy Syst*. 1995;10(3).
34. Borghetti A, Caldon R, Mari A, Nucci CA. On dynamic load models for voltage stability studies. *IEEE Trans Power Syst*. 1997;12(1, February).
35. Khlifi MA, Slimene MB, Fredj MB, Rehaoulia H. Performance evaluation of self-excited DSIG as a stand-alone distributed energy resource. *Springer Electr Eng*. 2016;97(4):261-345.
36. Karlsson D, Hill DJ. Modelling and identification of nonlinear dynamic loads in power systems. *IEEE Trans Power Syst*. 1994;9(1):157-163.
37. Leung Joseph S. K. and Hill D. J.. Coordinated power system security control, bulk power system dynamics and control – VI, August 22–27, 2004, Cortina d'Ampezzo, Italy.
38. Cutsem TV, Vournas C. *Voltage Stability of Electric Power Systems*. Klumer Academic Publishers; 1998.
39. Khlifi MA. Behavior of a dual stator induction machine fed by neutral point clamped multilevel inverter. *J Energy*. 2018, Article ID;2018:6968023. https://doi.org/10.1155/2018/6968023
40. Seydel R. *Practical Bifurcation and Stability Analysis: From Equilibrium to Chaos*. 2nd ed. New York: Springer-Verlag; 1994.
41. Khlifi MA, Rhaoulia H. General modelling of saturated AC machines for industrial drives. *COMPEL: Int J Comput Math Electr Electron Eng*. 2016;35(1):44-63.
42. Guo-Yun Cao, Li-Xia Liu, Liang Zhao，Chen C Continuation method to compute two-dimensional parameter local bifurcations boundary in power system stability differential-algebraic equation model, *Proc CSEE*，2005，25(8):13–16.
43. Dobson I., van Custem T., Vournas C. and Canizares C.A., Voltage stability assessment: concepts, practices and tools, IEEE Power Engineering Society, August 2002.
44. Kwatny HG, Fischl RF, Nwankpa C. Local bifurcation in power systems: theory, computation and application. In: Hill DJ, editor. Special issue on nonlinear phenomena in power systems: theory and practical implications. *IEEE Proc*. 1995;83(11):1456-1483.
45. Hiskens IA, Davy RJ. Exploring the power flow solution space boundary. *IEEE Trans Power Syst*. 2001;16(3):389-395.
46. Slimene MB, Khlifi MA. Performance limits of three-phase self-excited induction generator (SEIG) as a stand alone DER. *J Electr Eng Technol (JEET)*. 2017;12(1).
47. Li G, Yao Z, Yong-Qiang L. An extended equations method to compute two-dimensional parameter bifurcations boundary in power systems. *Relay*. 2006;34(12):20-24.

48. al Ahmadi S, Khlifi MA, Draou A. Voltage and frequency regulation for autonomous induction generators in small wind power plant. *Int J Adv Appl Sci*. 2019;6(1):95-98.

49. CIGRE Working Group C4.061, modeling and dynamic behavior of wind generation as it relates to power system control and dynamic performance, section 6, CIGRE, Tech Rep, Aug. 2007.

50. Abdelaziz Saïdi, Khadija Ben Kilani, Mohamed Elleuch. Dynamic stability of distribution network system with fixed speed wind power: a bifurcation analysis. IEEE International Conference on Electrical Engineering Design and technologies ICEEDT 2007.

How to cite this article: Saidi AS, Ben Slimene M, Khlifi MA, Fazle Azeem M, Al Ahmadi S, Draou A. Analysis and study of two-dimensional parameter bifurcation of wind power farms and composite loads. *Wind Energy*. 2019;1–17. https://doi.org/10.1002/we.2353

Appendix A.

Dynamic data of the DFIG[11]

Parameters	Descriptions	Values
P_n	Power rating	2 MW
V_n	Voltage rating	0.69 kV
F_n	Frequency rating	50 Hz
R_s	Stator resistance	0.01 pu
X_s	Stator reactance	0.1 pu
R_r	Rotor resistance	0.01 pu
X_r	Rotor reactance	0.08 pu
X_m	Magnetizing reactance	3 pu
H_m	Rotor inertia	3 s
K_p	Pitch control gain	1
T_p	Pitch control time constant	3 s
K_v	Voltage control gain	10
T_ε	Power control time constant	0.01 s
R	Rotor radius	75 m
P	Number of poles	4
n_b	Number of blades	3
η_{GB}	Gear box ratio	0.011236